Solid State Sciences 129 (2022) 106899

Contents lists available at ScienceDirect

Solid State Sciences

journal homepage: www.elsevier.com/locate/ssscie

# Study on the synthesis and properties of novel grass green oxides based on $Ba_4In_{2-x}Mn_xO_{7+y}$

Yuncheng Zhou [a,b], Qiuyu Cheng [a], Bin Li [a], Peng Jiang [a,*], Wenbin Cao [a], M.A. Subramanian [c]

[a] School of Materials Science and Engineering, University of Science and Technology Beijing, Beijing, 100083, China
[b] State Key Laboratory of Multiphase Complex Systems, Institute of Process Engineering, Chinese Academy of Sciences, Beijing, 100190, China
[c] Department of Chemistry, Oregon State University, Corvallis, OR, 97331, USA

ARTICLE INFO

*Keywords:*
Square pyramid coordination
Mn doping
Optical properties
*D-d* transition

ABSTRACT

A new solid solution based on general formula $Ba_4In_{2-x}Mn_xO_{7+y}$ ($0 \leq x \leq 0.2$) has been successfully synthesized by the sol-gel method. The compounds exhibited grass green to olive colors. The origin of the color apparently due to the presence of $Mn^{4+}$ as a chromophore in square pyramidal coordination. The X-ray diffraction results showed that the space group of all samples is *I4/mmm*. The oxidation state of Mn ion is confirmed to be +4 from the results of magnetization measurements and X-ray photoelectronic spectra (XPS). The color of $Ba_4In_2O_7$ is white. With a small amount of Mn substitution, the color of $Ba_4In_{2-x}Mn_xO_{7+y}$ solid solution changes to grass green, and it turned to olive green when $x = 0.2$. The UV–Vis absorbance spectra revealed that the absorption peaks are fitted with $d^3$ ($Mn^{4+}$) configuration in the square pyramid, and the mechanism of color is explained.

## 1. Introduction

The recent reports on the optical and pigment properties of $Ba_2In_{2-x}Mn_xO_{5+x}$ compounds have generated lot of interest in oxides containing barium and indium [1–3]. Among many Ba–In–O compositions, $Ba_4In_2O_7$ has attracted our interest due to a unique crystal structure, in which In ion is located in the square pyramid coordination as shown in Fig. 1. $Ba_4In_2O_7$ belongs to *I4/mmm* space group. Its crystal structure is based on corner-shared [$InO_5$] square pyramidal staggered sheets interleaved with B–O layers [4].

Only a few papers regarding $Ba_4In_2O_7$ have appeared in the literature. Golab et al. doped Nd and Er into $Ba_4In_2O_7$ by a solid-state reaction method to prepare luminescent materials [6]. Wang et al. used a sol-gel method to synthesize the Cr-doped $Ba_4In_2O_7/In_2O_3$ composite material for hydrogen storage alloy optical electrode [7]. The photocatalytic performance of $Ba_4In_2O_7$ prepared by the low-temperature combustion method was assessed by Zhang et al. [8]. But research on the other properties, especially optical properties, of $Ba_4In_2O_7$ has not yet been reported.

Due to the rarity of square pyramid coordination in oxides, very few papers have appeared in the literature where transition metal has been introduced as a chromophore in these structures to create durable color pigments when compared to the relatively common tetrahedral and trigonal bipyramidal coordination in transition metal oxides [9–13]. Unlike octahedral coordination, the square pyramid coordination belongs to the non-centrosymmetric structure, which is favored by the *d-d* transition due to the relaxation of selection rules. Fig. 2 shows the d-orbital splitting in an ideal square pyramid crystal field. Jazouli et al. prepared novel inorganic pigments present grey, orange, and cyan color with $Co^{2+}$, $Ni^{2+}$ and $Cu^{2+}$ doped in $SrZnP_2O_7$, among which the doped ions were in the [$ZnO_5$] square pyramids [14]. Jose et al. prepared $Y_2BaCuO_5$ green pigment with high infrared reflectance, and $Cu^{2+}$ was in the square pyramid coordination [15]. So, transition metal ion substitution into the five-fold square pyramid coordination will possibly bring intense colors to the oxides. $Ba_4In_2O_7$, in which all the In ions situated in the square pyramid coordination is therefore considered as a possible host for color generation in oxide which may lead to durable inorganic color pigments.

Mn is known to be a good chromophore in oxides as it can exhibit multiple oxidation states and adopt various coordinations. For example, $Mn^{3+}$ trigonal bipyramidal coordination in hexagonal $YIn_{1-x}Mn_xO_3$ resulting in vivid blue color or $Mn^{5+}$ in tetrahedral coordination in $Ba_2In_{2-x}Mn_xO_{5+x}$ turquoise to a green solid solution with brownmillerite structure [1,16]. Since the color, valence state, and optical properties of Mn ion in the square pyramid coordination have not yet reported, we attempted to dope Mn into the [$InO_5$] square pyramids in $Ba_4In_2O_7$

* Corresponding author.
*E-mail address:* jiangp@ustb.edu.cn (P. Jiang).

https://doi.org/10.1016/j.solidstatesciences.2022.106899
Received 6 March 2022; Received in revised form 19 April 2022; Accepted 21 April 2022
Available online 10 May 2022

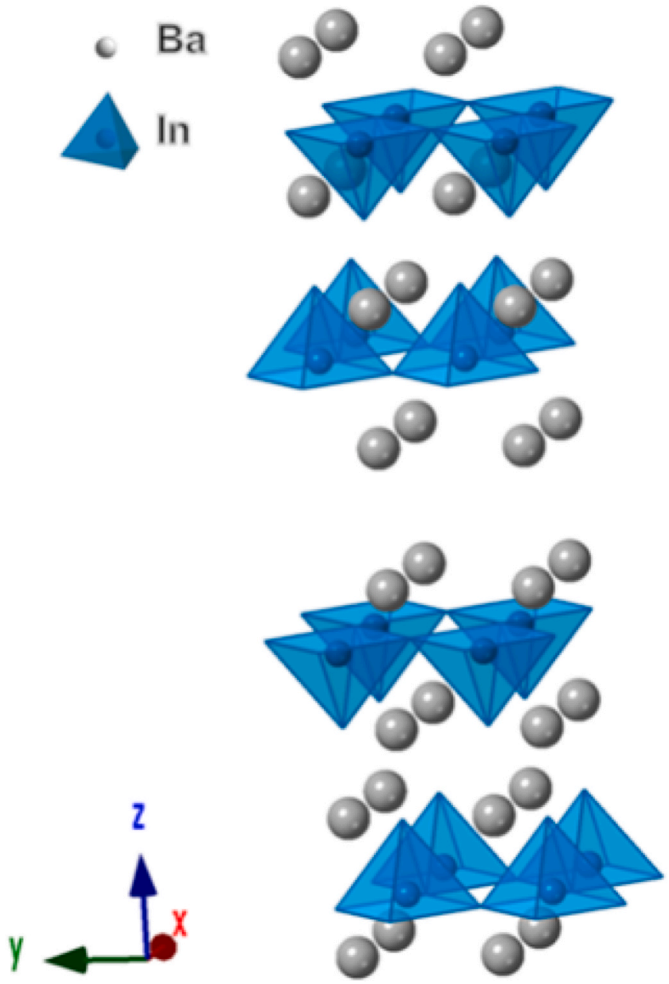


**Fig. 1.** The crystal structure of $Ba_4In_2O_7$ [5].

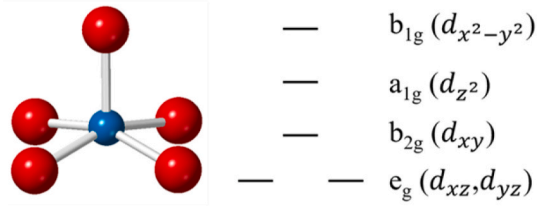


**Fig. 2.** The d-orbital splitting in an ideal square pyramid crystal field.

structure by a sol-gel method. The as-synthesized oxides turned to grass green to olive colors when a small amount of Mn is doped into the sites of $Ba_4In_2O_7$ structure. Our study conclude the presence of $Mn^{4+}$ in the square pyramid coordination is the root cause of the exhibited colors.

## 2. Experimental

### 2.1. Sample preparation

The synthetic procedure is shown in Fig. 3. The $Ba_4In_{2-x}Mn_xO_{7+y}$ ($0 \leq x \leq 0.2$) samples were prepared by a sol-gel method. $Ba(NO_3)_2$ (99.0% purity, Sinopharm Chemical Reagent Co, Ltd, China), $In(NO_3)_3{\cdot}4H_2O$ (99.99% purity, Energy Chemical, China), $Mn(NO_3)_2$ (wt50% purity, Sinopharm Chemical Reagent Co, Ltd, China), citric acid (99.0%, Aladdin, China) and $NH_3{\cdot}H_2O$ (30%, Sinopharm Chemical Reagent Co, Ltd, China) were used as starting reactants. All the nitrates were dissolved in deionized water by the stoichiometric proportion of objective products to form a transparent solution, and citrate acid was added to the solution with a molar ratio of citrate acid to the metal which equals 3:1. The pH of the solution was then adjusted to 10 using $NH_3{\cdot}H_2O$. The obtained transparent solution was kept in a 65 °C water bath with magnetic stirring to remove excess water and the mixture was converted to a claret transparent sticky gel, finally. The gel was dried at 160 °C for 12 h in air and the precursor was obtained. The precursor was heated at 600 °C for 1 h to remove the organic carbon. The resulting powder was well ground, spread in an alumina crucible, and calcined at 1000 °C for 12 h. One of the samples was later reduced in an $H_2$/Ar gas mixture (10% $H_2$) at 600 °C for 4 h.

### 2.2. Characterization

The powder X-ray diffraction (XRD) analysis of the samples were performed on a Bruker D8 Advance diffractometer with Ni-filtered Cu Kα radiation. The data were collected in a $2\theta$ range of 15–65° with an 8°/min scan speed.

The data were collected in a $2\theta$ range of 10–90° with a 1°/min scan speed. The relative content of the identified phases was calculated by quantitative phase analysis without standard fitting with multi-phase and full spectrum using the TOPAS 5 software (Bruker AXS, Karlsruhe, Germany) implementing the Rietveld method. Rietveld refinement using the XRD data by TOPAS 5.0 software allows to carefully determine the content of each phase. For all the Rietveld refinements in this work, the two important refinement parameters of the TOPAS 5.0 program, weighted residual factor ($R_{wp}$, %) and sigma value (S), were in the range of 8.35%–14.96% and 1.22–1.92, respectively, indicating reliable Rietveld refinements.

The oxidation state of the Mn in the compound was analyzed by magnetic analysis and X-ray photoelectron spectroscopy (XPS, ESCALAB 250XI). Magnetic data were collected [17] from a Quantum Design

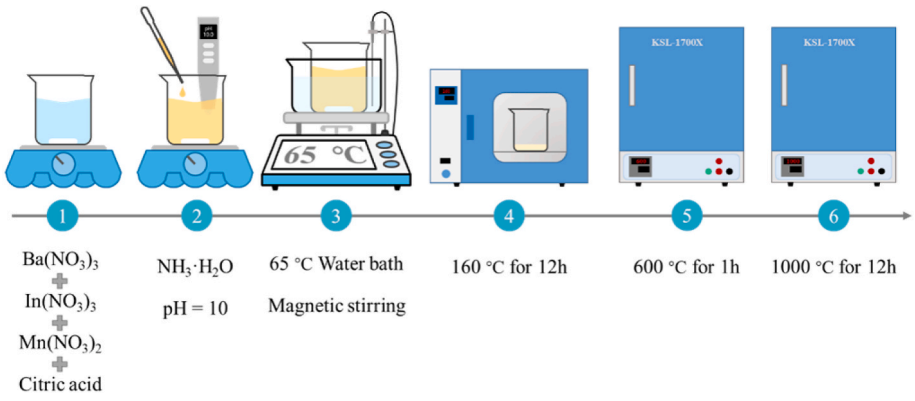


**Fig. 3.** Synthesis of $Ba_4In_{2-x}Mn_xO_{7+y}$ ($0 \leq x \leq 0.2$) pigment samples.

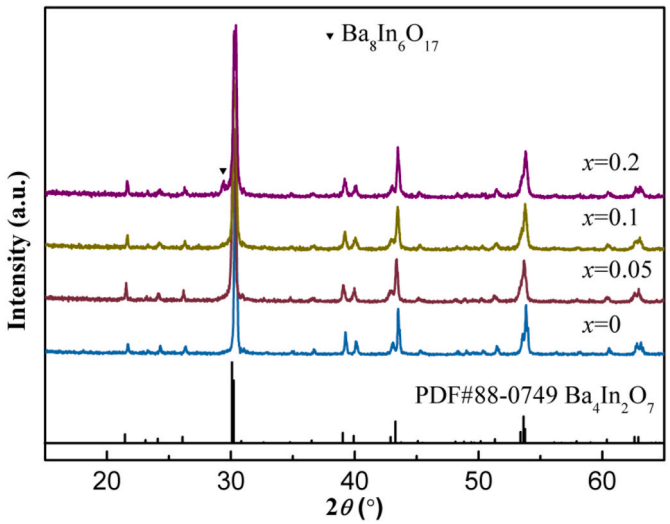


**Fig. 4.** X-ray diffraction patterns of $Ba_4In_{2-x}Mn_xO_{7+y}$ pigments.

SQUID-VSM over a temperature range of 5–300 K, using the zero-field cooling method with an applied magnetic field of 5000 Oe. Based on the $1/\chi_m$ vs. temperature graph, paramagnetic behavior can be detected in the measured temperature range (5–300 K) and obeys the Curie-Weiss law

$$\chi_m = C / (T + \theta)$$

where $C$ is the Curie constant, and $\theta$ is the Weiss constant. The experimental effective moment in the linear range (150–300 K) is calculated from equation

$$\mu_{eff}(exp) = \sqrt{\frac{3kC}{N_A}} = 2.84\sqrt{C}\mu_B$$

where $k$ is Boltzmann's constant, $C$ is the Curie constant, $N_A$ is Avogadro's number, and $\mu_B$ is the Bohr magneton, for both original and reduced samples, while the theoretical effective moment for the test sample is calculated from the equation

$$\mu_{eff}(th) = \sqrt{4xS(S+1)}\mu_B$$

where $x$ is Mn concentration which is confirmed from the XPS result to be 0.13 [10,17].

UV–Vis absorbance spectra were collected between 200 nm and 1300 nm at room temperature by a Hitachi UV–Visible/NIR Spectrophotometer (UH4150) with barium sulfate ($BaSO_4$) as a reference.

The CIE L*a*b* system was characterized using a 3 nhYS3060 grating spectrophotometer. The spectral range was from 400 nm to 700 nm with a D65 calibrated light source, and the complementary observer is 10° with a d/8° measurement geometry. In CIE L*a*b* system, L* represents the brightness (white (100) to black (0)), a* represents the red (>0) to green (<0) axis, and b* represents yellow (>0) to blue (<0) axis.

## 3. Results and discussion

### 3.1. X-ray diffraction analysis

The XRD patterns of the $Ba_4In_{2-x}Mn_xO_{7+y}$ ($0 \le x \le 0.2$) samples shown in Fig. 4 indicate that all the samples possess a tetragonal $Ba_4In_2O_7$ phase with the space group *I4/mmm* (PDF#88–0479), which demonstrate a successful synthesis of the solid solution. When $x$ is higher than 0.2, an impurity phase peak appears at 29.5°, which can be identified as a tetragonal phase of $Ba_8In_6O_{17}$ (PDF#42–0150). $Ba_8In_6O_{17}$ belongs to the *I4/mmm* space group and has similar lattice parameters to $Ba_4In_2O_7$, but the In ion in $Ba_8In_6O_{17}$ is located in [$InO_6$] octahedrons as shown in Fig. 5. Similar crystal structure and lattice parameters may be the cause of $Ba_8In_6O_{17}$ impurity appeared in $Ba_4In_{2-x}Mn_xO_{7+y}$ samples when $x$ is higher than 0.2.

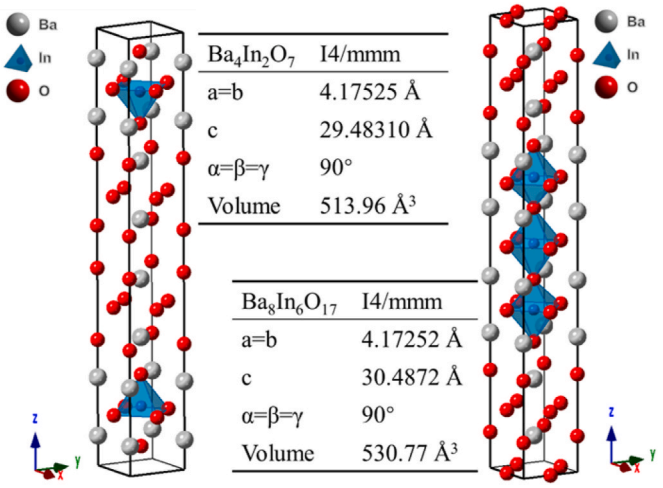


**Fig. 5.** Crystal structure and lattice parameters of $Ba_4In_2O_7$ (left) and $Ba_8In_6O_{17}$ (right) [5,18].

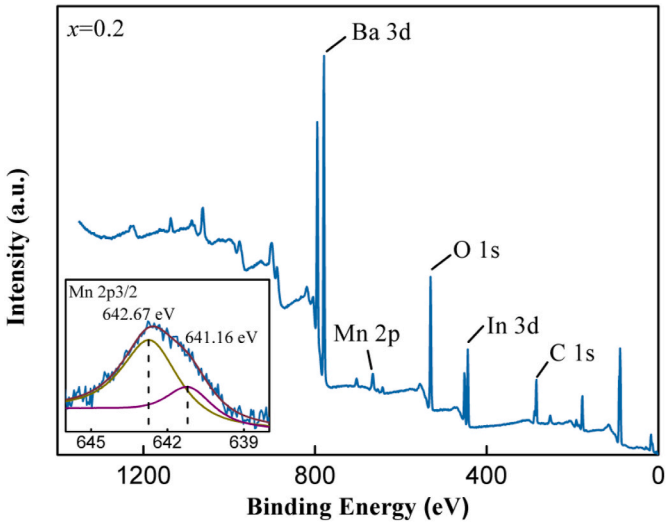


**Fig. 6.** X-ray photoelectron spectrum of $Ba_4In_{1.9}Mn_{0.1}O_{7+y}$.

### 3.2. XPS analysis

The valence state of Mn ions in the crystal field has an important effect on the color of oxides. Previous research has shown that $Mn^{3+}$ in trigonal bipyramidal coordination brings blue or purple color [16,19] while $Mn^{5+}$ in tetrahedron coordination presents turquoise-green color [20]. Therefore, it is necessary to confirm the valence state of Mn ion in $Ba_4In_{2-x}Mn_xO_{7+y}$ samples. The $Ba_4In_{1.9}Mn_{0.1}O_{7+y}$ sample was picked out to study the valence state of the Mn ion.

The full scan of the binding energy and a detailed profile analysis of the Mn $2p_{3/2}$ in $Ba_4In_{1.9}Mn_{0.1}O_{7+y}$ is shown in Fig. 6. The binding energy is corrected with the C 1s to compensate for the surface charge effects. For Mn $2p_{3/2}$ peak, the binding energy of 641.63 eV coincided with 641.6 eV for $Mn^{4+}$ in $MnO_2$ [21], which suggests that the valence state of Mn ion in the $Ba_4In_{1.9}Mn_{0.1}O_{7+y}$ should be +4.

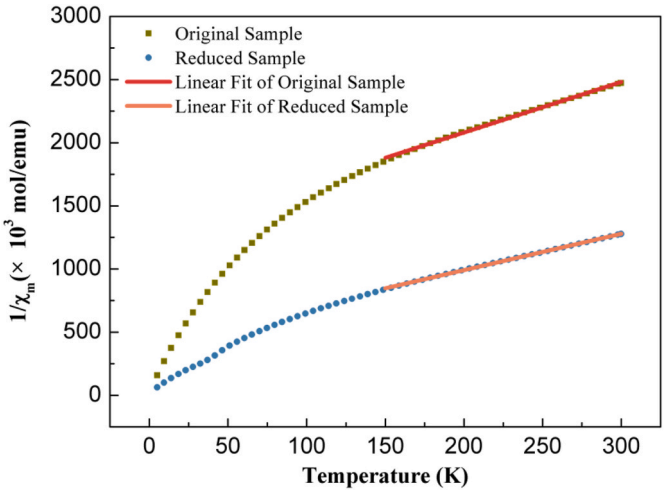


**Fig. 7.** Inverse magnetic susceptibility of $Ba_4In_{1.9}Mn_{0.1}O_{7+y}$ sample and reduced sample.

**Table 1**
Summary of magnetic data for as-prepared $Ba_4In_{1.9}Mn_{0.1}O_{7+y}$ sample and after reduction.

| Experimental value | | | | Theoretical value | | |
|---|---|---|---|---|---|---|
| Sample | $T$ (K) | $C$ | $\mu_{eff}$ ($\mu B$) | $Mn^{n+}$ | $S$ | $\mu_{eff}$ ($\mu B$) |
| Original | 150–300 | 0.2497 | 1.419 | $Mn^{2+}$ | 5/2 | 2.182 |
| | | | | $Mn^{3+}$ | 4/2 | 1.807 |
| Reduced | 150–300 | 0.3475 | 1.674 | $Mn^{4+}$ | 3/2 | 1.428 |
| | | | | $Mn^{5+}$ | 2/2 | 1.043 |

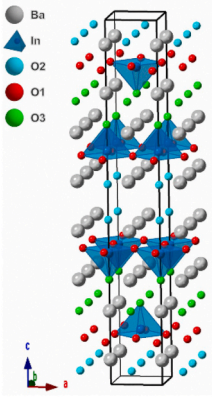


| Site | Atom | $x$=0 | | $x$=0.05 | | $x$=0.1 | |
|---|---|---|---|---|---|---|---|
| | | Occ. | $U_{iso}$ | Occ. | $U_{iso}$ | Occ. | $U_{iso}$ |
| Ba1 | Ba+2 | 1 | 0.62(5) | 1 | 0.65(9) | 1 | 0.72(7) |
| Ba2 | Ba+2 | 1 | 0.54(7) | 1 | 0.59(7) | 1 | 0.65(4) |
| In1 | In+3 | 1 | 0.35(6) | 0.975 | 0.24(9) | 0.95 | 0.02(9) |
| | Mn+3 | - | - | 0.025 | 0.10(4) | 0.05 | 0.14(0) |
| O2 | O-2 | 0.5 | 1.44(0) | 0.5 | 0 | 0.5 | 0 |
| O1 | O-2 | 1 | 0.62(0) | 1 | 2.37(6) | 1 | 0 |
| O3 | O-2 | 1 | 0.76(0) | 1 | 0 | 1 | 0 |

**Fig. 8.** Crystal structure of $Ba_4In_2O_7$ and the simplified final Rietveld refinement parameters.

### 3.3. Magnetic properties

To further determine the valence state of Mn ion in $Ba_4In_{1.9}Mn_{0.1}O_{7+y}$, magnetic studies were performed using SQUID-VSM. Considering the effect of the valence state of Mn ion on color, the sample was reduced under $H_2$/Ar at 600 °C. Magnetic properties of the typical sample $Ba_4In_{1.9}Mn_{0.1}O_{7+y}$ and the reduced sample are plotted in Fig. 7 and the relevant magnetic data are listed in Table 1. Thus, the experimental $\mu_{eff}$ (exp) value of the original sample 1.419$\mu_B$ is close to 1.428$\mu_B$, indicating the presence of Mn as $Mn^{4+}$ [($d^3$) in high spin configuration] in $Ba_4In_{1.9}Mn_{0.1}O_{7+y}$ samples. When the sample with $x = 0.1$ is reduced in hydrogen, the sample turned to brownish color. And the experimental $\mu_{eff}$ (exp) value 1.674$\mu_B$ is between the theoretical $\mu_{eff}$ (th) of $Mn^{3+}$ and $Mn^{4+}$, which implies that the sample is successfully reduced and the

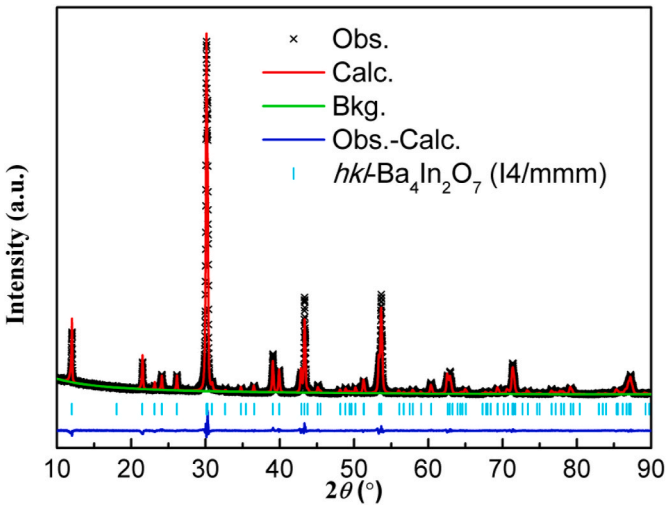


**Fig. 9.** Refinements of $Ba_4In_{1.95}Mn_{0.05}O_{7+y}$ using the Rietveld method.

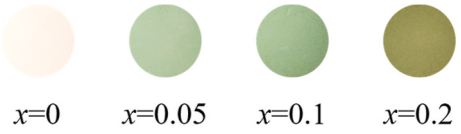


**Fig. 10.** Apparent colors of $Ba_4In_{2-x}Mn_xO_{7+y}$. *(For interpretation of the references to color in this figure legend, the reader is referred to the Web version of this article.)*

oxide state of Mn in the original sample should be higher than +3. Combined the magnet moment calculation with the XPS data, we confirm the valence state of Mn ion in $Ba_4In_{1.9}Mn_{0.1}O_{7+y}$ is +4.

### 3.4. XRD refinements analysis

According to the results of XPS and SQUID-VSM, the valence state of Mn in the matrix is +4. To balance the oxidation state of the compound, excess oxygen may be introduced into the structure. Therefore, the XRD data of samples with $x = 0$, 0.05, and 0.1 were refined by the Rietveld method to confirm the existence and position of excess oxygen. The refined crystal structure of $Ba_4In_2O_7$ (space group *I4/mmm*) and the simplified final Rietveld refinement parameters are shown in Fig. 8. The refined plot of $Ba_4In_2O_7$ and $Ba_4In_{1.95}Mn_{0.05}O_{7+y}$ is provided in Figure S1 and Fig. 9, respectively, and detailed final Rietveld refinement parameters are given in Table S1-S3. According to the refined results, the movement of oxygen is greatly affected by the introduction of Mn. The $U_{iso}$ values of O1, O2, and O3 show a giant change compared to $Ba_4In_2O_7$. O1, which locates in the four corners of the square pyramidal coordination, increases to 2.37 from 0.62, indicating a wider range of movement. And the two oxygen atoms along the c axis (O2 and O3) turn out to be very small (close to 0). This may be a result of the shift from its initial position. So, a possible position for the excess oxygen brought by $Mn^{4+}$ should be located along the same axis as O2 and O3. Due to the small substitution amount of Mn, the detailed position of this excess oxygen is too difficult to be determined. In the case of the sample with $x = 0.1$, the $U_{iso}$ values of three oxygen atoms (O1, O2, and O3) became almost 0 which indicates more distorted coordination. As a result of this change, the polyhedra may transit to octahedra. And that may explain the fact that with a higher amount of Mn ($x = 0.2$), the impurity of $Ba_8In_6O_{17}$ appears.

### 3.5. Optical properties

The colors of the prepared $Ba_4In_{2-x}Mn_xO_{7+y}$ samples are shown in Fig. 10. The undoped sample presents a white color. With low Mn

**Table 2**
The CIE L*a*b* color coordinates of the $Ba_4In_{2-x}Mn_xO_{7+y}$ pigments.

| x | L* | a* | b* | Color |
|---|---|---|---|---|
| 0 | 95.05 | −0.83 | 5.17 | |
| 0.05 | 75.24 | −12.77 | 11.83 | |
| 0.1 | 69.03 | −12.6 | 11.73 | |
| 0.2 | 55.11 | −5.37 | 13.45 | |

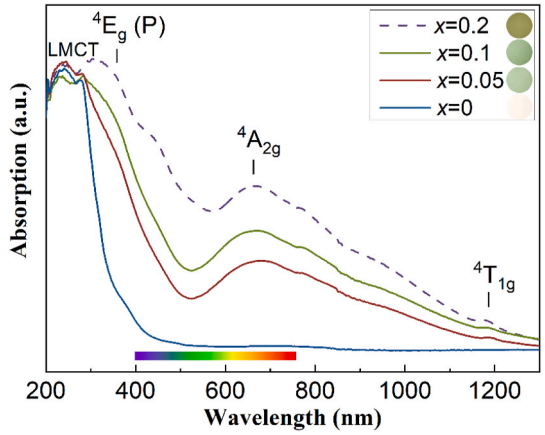


**Fig. 11.** UV–Vis absorbance spectra of $Ba_4In_{2-x}Mn_xO_{7+y}$.

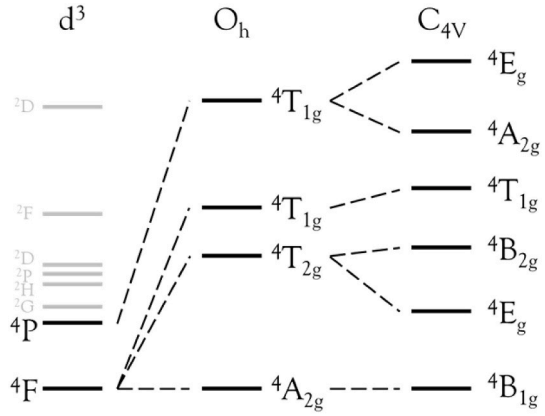


**Fig. 12.** The spectroscopic term of $d^3$ with the high spin configuration in the square pyramid field.

doping amount ($x = 0.05, 0.1$), the samples present grass-green, while the sample turned olive-green when $x = 0.2$.

The CIE color coordinates and the analog colors of the pigments are listed in Table 2. We can see that the colors changed from white ($x = 0$, $a^* \approx 0$, $b^* > 0$) to grass green ($x = 0.05, 0.1$, $a^* < 0$, $b^* > 0$). With more Mn doping amount ($x = 0.2$), the pigment absorbs more blue and green region photons, which increases the value of a* and b* and turns the color into olive green.

The UV–Vis absorbance spectra are shown in Fig. 11. The undoped sample barely absorbs photon energy in the visible region. With the doping of Mn ion, $Ba_4In_{2-x}Mn_xO_{7+y}$ showed an obvious absorption peak in the visible region, and the absorption intensity increases with the elevated doping amount. Four peaks were found with low Mn-doped samples ($x = 0.05, 0.1$): at about 210, 368, 662, 1186 nm. The peak at 210 nm is mainly due to a ligand-to-metal charge-transfer (LMCT) transition. The rest three peaks are attributed to the d-d transition of the Mn ion. Although there is no literature research on the $Mn^{4+}$ with the high spin configuration in the square pyramidal crystal field, the square pyramidal crystal field can be treated as an octahedral with tetragonal distortion [14]. Based on the spectroscopic term of $d^3$ in the octahedral crystal field, we can get the spectroscopic term of $d^3$ with the high spin configuration in the square pyramidal crystal field as shown in Fig. 12. This tetragonal distortion leads to the transformation of the fundamental level $^4A_{2g}$ term into $^4B_{1g}$ term, the splitting of the $^4T_{2g}$ term into $^4B_{2g}$ and $^4E_g$ terms, the $^4T_{1g}$(F) term remaining a singlet, the splitting of the $^4T_{1g}$(P) term into $^4E_g$(P) and $^4A_{2g}$(P) terms. Hence, in the energy growing order, five peaks are anticipated from the fundamental level which are $^4B_{1g}$ to $^4E_g$, $^4B_{2g}$, $^4T_{1g}$(F), $^4A_{2g}$(P), and $^4E_g$(P) levels. Both of $^4E_g$ and $^4B_{2g}$ levels in the far-infrared region are not fully accessible from our spectrometer and the three other peaks are indexed in Fig. 11. The absorbance curves have some differences between low Mn doping amount (solid lines) and high amount (dash line) in Fig. 11, this might be due to the formation of $Ba_8In_6O_{17}$ impurity, in which Mn might locate in both distorted square pyramidal and octahedral coordination.

## 4. Summary and conclusions

In this work, we have successfully synthesized the $Ba_4In_{2-x}Mn_xO_{7+y}$ grass green pigments through a simple sol-gel method. The XRD results confirmed that $Ba_4In_{2-x}Mn_xO_{7+y}$ samples are single phase. Based on the magnetic properties and XPS analysis, Mn ion is +4 oxidation state in these compounds. The presence of $Mn^{4+}$ in $[InO_5]$ distorted square pyramid sites in $Ba_4In_2O_7$ is responsible for the grass green to olive colors observed in this solid solution.

## Author statement

**Peng Jiang** proposed the overall research direction and guided the project. **Peng Jiang** and **Yuncheng Zhou** conceived the idea and designed the experiments, performed the materials synthesis, analyzed data, and drafted the manuscript. **Qiuyu Cheng** helped to draft the manuscript. **Bin Li** contributed to the Rietveld refinement. Wenbin Cao and M. A. Subramanian gave valuable discussions and suggestions.

## Declaration of competing interest

The authors declare that they have no known competing financial interests or personal relationships that could have appeared to influence the work reported in this paper.

## Acknowledgments

This work was supported by the National Natural Science Foundation of China under Grant No. 51872023; and Fundamental Research Funds for the Central Universities and the Youth Teacher International Exchange & Growth Program under the grant No. FRF-MP-20-28and No. QNXM20210020. The work done at Oregon State University is supported by US National Science Foundation Grant No. DMR-2025615.

## Appendix A. Supplementary data

Supplementary data to this article can be found online at https://doi.org/10.1016/j.solidstatesciences.2022.106899.

## References

[1] P. Jiang, J. Li, A. Ozarowski, A.W. Sleight, M.A. Subramanian, Intense turquoise and green colors in brownmillerite-type oxides based on $Mn^{5+}$ in $Ba_2In_{2-x}Mn_xO_{5+x}$, Inorg. Chem. 52 (2013) 1349–1357.
[2] P. Jiang, W. Yang, Y. Zhou, J. Kuang, Y. Li, T. Xiao, Synthesis and optical properties of turquoise- and green-colored brownmillerite-type $Ba_2In_{2-x-y}Mn_xAl_yO_{5+x}$ codoped with manganese and aluminum, International Journal of Minerals, Metallurgy, and Materials 23 (2016) 1346–1351.

[3] P. Jiang, T. Xiao, Y. Zhou, J. Kuang, Q. Wang, W. Cao, Facile synthesis of brownmillerite-type oxides $Ba_2In_{2-x}Mn_xO_{5+x}$ through a microwave-assisted process, Solid State Sci. 65 (2017) 1–5.
[4] P. Villars, K. Cenzual, J. Daams, R. Gladyshevskii, R. Zaremba, $Ba_4In_2O_7$, Structure Types. Part 10: Space Groups (140) I4/mcm-(136) P42/mnm 2011.
[5] A. Lalla, Müller-Buschbaum, Über das Oxoindat $Ba_4In_2O_7$, Z. Anorg. Allg. Chem. 573 (1989) 12–18.
[6] S. Gołąb, A. Zygmunt, W. Ryba-Romanowski, Synthesis and emission spectra of $Ba_4In_{1.98}Nd_{0.02}O_7$ and $Ba_4In_{1.98}Er_{0.02}O_7$, J. Alloys Compd. 300–301 (2000) 295–299.
[7] X.L. Wang, J.P. Tu, S.F. Wang, Y.F. Yuan, K.F. Li, J. Zhang, Preparation of Cr-doped $Ba_4In_2O_7/In_2O_3$ nanocomposite and its photo-assisted chargeability in hydrogen storage alloy/photocatalyst electrode, J. Alloys Compd. 462 (2008) 220–224.
[8] Q. Zhang, B. Yao, C. Peng, L. Sun, Self-propagating combustion synthesis of $Ba_4In_2O_7$ and its photocatalytic activity, Chin. J. Mater. Res. 29 (2015) 39–44.
[9] S. Laha, S. Tamilarasan, S. Natarajan, J. Gopalakrishnan, Stabilization of a tetrahedral ($Mn^{5+}O_4$) chromophore in ternary barium oxides as a strategy toward development of new turquoise/green-colored pigments, Inorg. Chem. 55 (2016) 3508–3514.
[10] P. Jiang, J. Li, A.W. Sleight, M.A. Subramanian, New oxides showing an intense orange color based on $Fe^{3+}$ in trigonal-bipyramidal coordination, Inorg. Chem. 50 (2011) 5858–5860.
[11] H.R. Hedayati, A.A. Sabbagh Alvani, H. Sameie, R. Salimi, S. Moosakhani, F. Tabatabaee, A. Amiri Zarandi, Synthesis and characterization of $Co_{1-x}Zn_xCr_{2-y}Al_yO_4$ as a near-infrared reflective color tunable nano-pigment, Dyes Pigments 113 (2015) 588–595.
[12] S.W. Kim, Y. Saito, T. Hasegawa, K. Toda, K. Uematsu, M. Sato, Development of a novel nontoxic vivid violet inorganic pigment-$Mn^{3+}$-doped $LaAlGe_2O_7$, Dyes Pigments 136 (2017) 243–247.
[13] M. Llusar, E. García, M.T. García, C. Gargori, J.A. Badenes, G. Monrós, Stability and coloring properties of Ni-qandilite green spinels (Ni, $Mg)_2TiO_4$: the "half color wheel" of Ni-doped magnesium titanates, Dyes Pigments 122 (2015) 368–381.
[14] A. El Jazouli, B. Tbib, A. Demourgues, M. Gaudon, Structure and colour of diphosphate pigments with square pyramid environment around chromophore ions ($Co^{2+}$, $Ni^{2+}$, $Cu^{2+}$), Dyes Pigments 104 (2014) 67–74.
[15] S. Jose, A. Prakash, S. Laha, S. Natarajan, M.L. Reddy, Green colored nano-pigments derived from $Y_2BaCuO_5$: NIR reflective coatings, Dyes Pigments 107 (2014) 118–126.
[16] A.E. Smith, H. Mizoguchi, K. Delaney, N.A. Spaldin, A.W. Sleight, M. A. Subramanian, $Mn^{3+}$ in trigonal bipyramidal coordination: a new blue chromophore, J. Am. Chem. Soc. 131 (2009) 17084–17086.
[17] F. Wan, X. Bai, K. Song, X. Lin, X. Han, J. Zheng, C. Cao, Structure and magnetism of Cr-doped h-$YMnO_3$, J. Magn. Magn Mater. 424 (2017) 371–375.
[18] K. Mader, H. Müller-Buschbaum, Synthese und kristallstruktur eines neuen oxoindats der zusammensetzung $Ba_8In_6O_{17}$, J. Less Common Met. 157 (1990) 71–76.
[19] S. Tamilarasan, D. Sarma, M.L.P. Reddy, S. Natarajan, J. Gopalakrishnan, $YGa_{1-x}Mn_xO_3$: a novel purple inorganic pigment, RSC Adv. 3 (2013).
[20] Y. Zhou, P. Jiang, H. Lei, Y. Li, W. Cao, J. Kuang, Synthesis and properties of novel turquoise-green pigments based on $BaAl_{2-x}Mn_xO_{4+y}$, Dyes Pigments 155 (2018) 212–217.
[21] B.V. Crist, Handbook of Monochromatic XPS Spectra: the Elements of Native Oxides, Wiley, Weinheim, 2000.